Machine learning model of acoustic signatures: towards digitalised thermal spray manufacturing.

VISWANATHAN, V., MCCLOSKEY, A., MATHUR, R., NGUYEN, D.T., FAISAL, N.H., PRATHURU, A., LLAVORI, I., MURPHY, A., TIWARI, A., MATTHEWS, A., AGRAWAL, A. and GOEL, S.

2024

Mechanical Systems and Signal Processing 208 (2024) 111030

Contents lists available at ScienceDirect

Mechanical Systems and Signal Processing

journal homepage: www.elsevier.com/locate/ymssp

Machine learning model of acoustic signatures: Towards digitalised thermal spray manufacturing

V. Viswanathan [a], Alex McCloskey [b], Ruchir Mathur [a], Dinh T. Nguyen [a], Nadimul Haque Faisal [c], Anil Prathuru [c], Iñigo Llavori [b], Adrian Murphy [d], Ashutosh Tiwari [e], Allan Matthews [f], Anupam Agrawal [g], Saurav Goel [a,h,*]

[a] School of Engineering, London South Bank University, 103 Borough Road, London SE1 0AA, UK
[b] Mechanical and Industrial Manufacturing Department, Mondragon Unibertsitatea, Loramendi 4, 20500 Arrasate-Mondragon, Spain
[c] School of Engineering, Robert Gordon University, Garthdee Road, Aberdeen AB10 7GJ, UK
[d] School of Mechanical and Aerospace Engineering, Queen's University, Belfast BT95AH, UK
[e] Department of Automatic Control and Systems Engineering, The University of Sheffield, S1 3JD, UK
[f] Henry Royce Institute, The University of Manchester, Manchester M13 9PL, UK
[g] Mays Business School, Texas A&M University, College Station, TX, USA
[h] Department of Mechanical Engineering, University of Petroleum and Energy Studies, Dehradun 248007, India

ARTICLE INFO

Keywords:
Thermal spray
Acoustic
Digitalisation
Machine learning

ABSTRACT

Thermal spraying, an important industrial surface manufacturing process in sectors such as aerospace, energy and biomedical, remains a skill intensive process often involving multiple trial runs impacting the yield. The core research challenge in digitalisation of thermal spraying process lies in instrumenting the manufacturing platform as the process includes harsh conditions, including UV Rays, high-plasma temperature, dusty chemical environment, and spray booth inaccessibility. This paper introduces a novel application of machine learning to the acoustic emission spectra of thermal spraying. By transitioning from the amplitude-time domain to a Fourier-transformed frequency-time domain, it is possible to predict anomalies in real-time, a crucial step towards sustainable material and manufacturing digitalization. Our experimental results also indicate that this method is suitable for industrial applications by generating useful data that can be used to develop Visual Geometry Group (VGG) transfer learning models to overcome the traditional limitations of convoluted neural networks (CNN).

1. Introduction

Thermal spraying dominates the surface manufacturing landscape as a special process for high technology sectors such as power generation, defense, bio medical and aerospace [1–4]. Despite its dominance, the process still relies heavily on strict manufacturing plans and work instructions to ensure quality and consistency. When post-coating analyses uncover non-compliant properties, it often leads to resource-intensive rework.

* Corresponding author at: School of Engineering, London South Bank University, 103 Borough Road, London SE1 0AA, UK.
E-mail address: Goels@lsbu.ac.uk (S. Goel).

https://doi.org/10.1016/j.ymssp.2023.111030
Received 17 August 2023; Received in revised form 7 November 2023; Accepted 11 December 2023
Available online 19 December 2023

1.1. Digitalisation of thermal spraying

Digitalised thermal spraying [5] is an important new area of research that could help in improving quality and reducing rework in this process. The first step towards digitising thermal spraying would be to collect the process data in a digital format. Extant research [6–8] provides insights into some of these aspects using computational fluid dynamics to reveal combustion models in relation to process parameters. However, the quest for a comprehensive in-situ sensor system for holistic coating quality monitoring remains a challenge. The need for diagnostics arises from the need for thermal spray processes to achieve coating homogeneity in terms of thickness, microstructure, and mechanical properties. In general, diagnostics primarily revolve around in-flight particle velocity and temperature measurements. Measurement of individual particle parameters include diagnostics with DPV 2000^{TM} and spray position trajectory sensor, Accuraspray^{TM}, Spraywatch^{TM}, Inflight Particle Pyrometer (IPP), particle image velocimetry (PIV) [9]. These sensors measure temperatures using IR emission emanating from molten particles and use time of flight to determine the particle velocities. Velocity can be precisely measured, but particle temperature readings could be inaccurate due to the uncertain emissivity of the material in a partially molten state. Moreover, substrate particle interaction could only be guessed based on the particle inflight diagnostics, which forms the basis of the microstructure and mechanical properties. Thus, in flight diagnostics may present certain disadvantages when compared to acoustic sensors. Moreover, inflight diagnostics are quite invasive when it comes to manufacturing factories' inclination to spend time and material only on the coating process and not for everyday diagnostics. Thus, acoustics sensors are well placed non-invasive sensors. However, development of contactless sensors suitable for high-temperature environments would help make the monitoring process more manufacturing-friendly.

Ideally, a sensor setup that could capture process deviations, displayed digitally on the shop floor, could provide a critical first step to digitalisation. The second step would be to develop machine learning models like Artificial Neural Networks (ANN) or Convolutional Neural Networks (CNN) to create a learning pattern for responsive manufacturing.

1.2. Using acoustic wave spectra in high temperature manufacturing

Electromagnetic and acoustic wave spectra can be used to monitor high temperature flying matter. The acoustic spectra encompass infrasound (<20 Hz), audible (20 Hz-20 kHz), and ultrasound (>20 kHz) frequencies [10]. Acoustic waves, generated when solid objects interact, have historical applications from infrastructure maintenance, as in assessing bridge durability from passing vehicles, to solving firearm-related crimes through noise analysis. Ultrasound, another application, is used to monitor foetal development. These applications typically operate at room temperature. Using acoustic monitoring in high-temperature processes like thermal spraying can streamline the need for multiple sensors and offer an integrated view of the process. An active application for the audible range is to identify in-situ mechanical behaviour of materials. Our study delves into the spectral analysis of particles impacting the substrate, probing the feasibility of detecting anomalies in feed rates, robot speeds, and surface preparation. For example, our spectral data suggest the potential to discern if a robot sprayed a component at a 90-degree angle or deviated from it. While several promising automation processes have been proposed in extant research on thermal spraying such as robot path optimisation [11] and parameter monitoring and control [12], acoustic emission is an interesting field of study for digitalisation of thermal spraying and even additive manufacturing methods.

1.3. Deep learning and transfer learning in high temperature manufacturing

Manufacturing is witnessing a transformative shift due to the rising adoption of deep learning models, particularly in process monitoring, defect detection, and predictive analytics [13–15]. Among these models, Convolutional Neural Networks (CNNs) are specially tailored to extract meaningful data from digital images, facilitating tasks like image classification. Yet, implementing CNNs or other deep learning tools in manufacturing isn't without challenges. One major hurdle is gathering a large, diverse training dataset [16].

Another concern is ensuring the long-term relevance of a model, especially in the ever-evolving industrial landscape. Transfer learning [17] emerges as a solution to these challenges. It allows CNN models to be trained on one dataset (source) and then adapted for another (target), thereby optimizing resources. In the context of manufacturing, it means using data from a range of production processes to build efficient models for specific applications. The Visual Geometry Group (VGG-16) model, developed by the University of Oxford [18], exemplifies this approach, using pre-trained CNN for transfer learning and serves as an important element in our research.

Overall, our research highlights the potential of acoustic wave spectra for monitoring high-temperature processes, such as thermal spraying, and introduces how deep learning models, such as CNNs, can be used in the high temperature manufacturing domain. We also highlight the significance of transfer learning, exemplified by the VGG-16 model, as a solution to the challenges faced in implementing deep learning in dynamic industrial settings.

2. Principle of acoustic emission

When a solid material gets bombarded with metal particles ranging in size from 50 to 100 μm, strain energy is released, producing elastic waves within the material. These waves emit from the point of impact and travel across the material, serving as valuable signals for process monitoring—these signals are known as acoustic emissions. Two main signal analysis methods are utilized: the parameter analysis method and the waveform analysis method. The former uses acoustic emission parameters to analyse the signals, while the

latter uses time domain waveforms and is more popular. Wavelet analysis combines the advantage of signal in the time domain and frequency domain [19].

If the particles were simply bombarded at room temperature without any melting or with a high temperature plasma involved, the resultant wave's characteristics differ based on the molten state of the particle - whether molten, unmolten or semi molten. Any anomaly that happens in the thermal spray process would be in between the window of a perfectly optimised molten droplet and a particle at room temperature. Each particle state has its distinct acoustic signature. Some acoustic emission events, such as an indentation during hardness testing, are so discrete, that one can capture signal amplitude vs time and then distinctly categorize them as being in a plastic zone or elastic zone.

In the case of thermal spray, where particles with different thermal states (molten, semi molten or unmolten) strike the substrate at different velocities, several such events gets recorded. So instead of studying the amplitude vs time domain, Fourier transformed frequency vs time domain is more suitable to understand the process parameters and the associated particle states. When hundreds of thousands of particles impact a surface, as in thermal spraying (see Fig. 1), the frequency distribution of particles can be examined, which can provide insights into process deviations.

3. Research methodology

An experimental approach was adopted, and a careful experimental plan was made to study the generation and propagation of acoustic waves in a steel substrate. A commercially available powder of Pure Titanium (Metco 4012A) in the angular form was deposited with F4 plasma spray gun with the spray parameters listed in Table 1. The particle size of the powder was in the range of 45–106 μm. Table 2 reveals the grit blasting parameters.

The data acquisition module comprised an acoustic emission kit with a 12-bit data acquisition board (BNC-2110, NI, UK) and a piezoelectric sensor made up of lead zirconate titanate (Micro-80D, PAC, UK) [20]. The kit consists of a preamplifier (1220A, Mistras UK). A sensor of about 12 mm height and 10 mm diameter was glued to the back of the steel base material (about 2 mm in thickness) with silicone grease as a transmitting medium secured with aluminium tape.

The preamplifier was set at 60 dB gain and was equipped with an internal band pass filter between 0.1 and 1 MHz. AE was recorded over the frequency range of 0.1 to 1 MHz with a sampling rate of 2.5 MHz and each recording was about 10–20 s long until the robot completes the raster and moves out of the spray sample.

The location of the sensor was at least 100 mm away from the spray path. The temperature of the plate never reached the temperature limit of the sensor during spraying. This was confirmed through a FLIR^{TM} (TL540 model) IR imaging camera. The specimen and the sensor configuration are shown in Fig. 2.

The spray gun was moved at a predetermined distance at 90° and 60°gun angles. The sensors used were Micro-80D broadband sensors supplied by physical acoustics corporation. The frequency response band of the sensors was between 100 kHz and 900 kHz. It is to be noted that the sensor can detect frequencies lower than 100 kHz, however, the response in these frequencies is poorer compared to that in the response band. The sensors were connected to 2/4/6 preamplifiers with an amplification of 20 dB. These pre-amplifiers are in turn connected to a BNC block which connects to the NI-6115 data acquisition card (DAQ) hosted on a computer. LabView software was used to create a visual interface to set the data acquisition parameters and to store the sensor generated data. The sampling rate during thermal spraying was set to 2 MHz. The raw data was extracted in the TDMS file format recording signal amplitude as a function of time. Due to the large volume of data, Python 3.0 was used to convert the TDMS to CSV files and split the

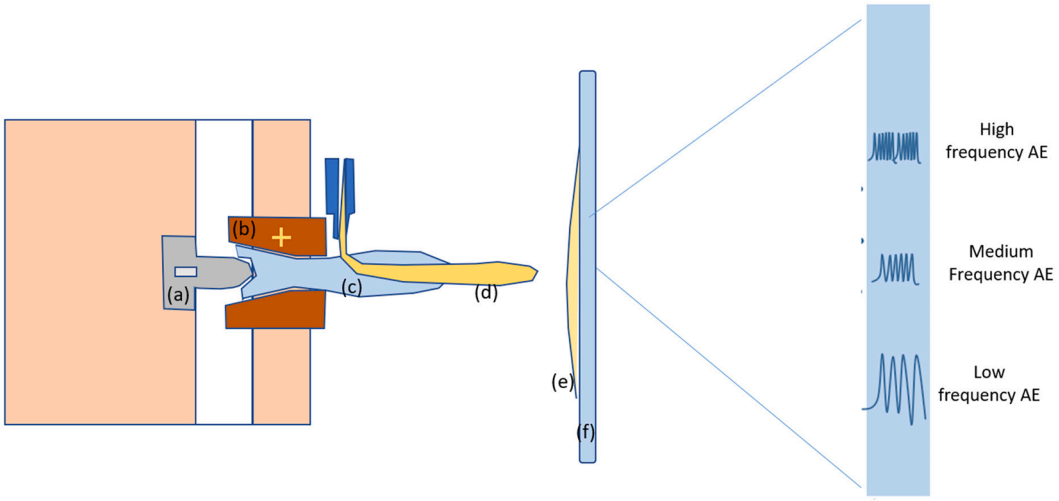

Fig. 1. Schematic of plasma spray gun cross section with the (a) electrode, (b) nozzle generating the (c) plasma plume which melts the (d) powder that becomes a (e) coating laid onto a (f) substrate. The impact of particles during the thermal spray process triggers many acoustic emission events which can have multiple frequencies depending on several factors.

Table 1
Spray parameters used for the acoustic emission experiments.

Powder name (Vendor Oerlikon)	Titanium Metco 4012 A
Gun Current	550 Amps
Voltage	18 Volts
Primary Gas (Argon)	50 slpm
Spray Distance	100 mm
Carrier Gas (argon)	6 slpm carrier
Hopper pressure	415 kPa
Blasting	Grit blasted @ 400 MPa with 24 grits. Some samples were intentionally used unblasted.
Microns/ pass Thickness Build up	10 μm per pass
Coating Pass Counts, Powder feed rate and robot speed	Varied as per the experimental plan (See S1 and S2 for supplementary information)

Table 2
Grit blasting parameters.

Blaster Model	Guyson DC 80
Grit Media	Brown Aluminium Oxide
Mesh Size	24
Blast Pressure	0.413 MPa
Blast angle	60 degrees

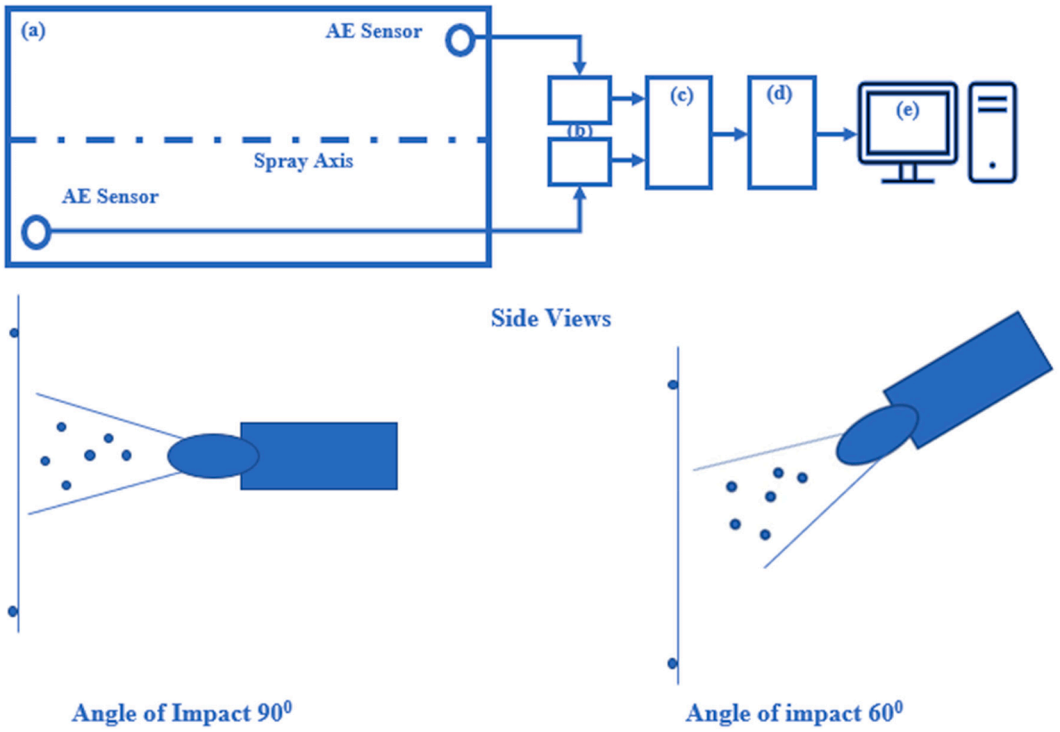

Fig. 2. Spray data acquisition layout revealing (a) backside of the steel plate on which the acoustic sensors were mounted, (b) amplifiers, (c) BNC blocks channelling the amplified data to (d) NI 6115 data acquisition card which connects to (e) the PC. The side views show two different gun angles being studied with respect to the plane of coating surface.

CSV files into processable data, with MATLAB. This was converted to time vs frequency plots to better understand the impact of particles on the plate because of such effects mentioned in the above table.

Four sets of conditions were chosen to be analysed as shown in Fig. 3. These conditions were 1) the effect of robot speed changes, 2) the effect of grit blasting vs no grit blasting of the substrate 3) the effect of change in powder feed and 4) the effect of change in gun angle i.e. 90° and 60° gun angle.

Table S1 and S2 provided as supplementary information shows the spray parameters matrix used in this investigation to understand the influence of processing on the acoustic signature during spraying. With all other parameters remaining constant, plasma spray gun F4 was used with the Unicoat controller. The ABB manipulator was used with an Oerlikon Metco 9MP feeder for spraying. Titanium

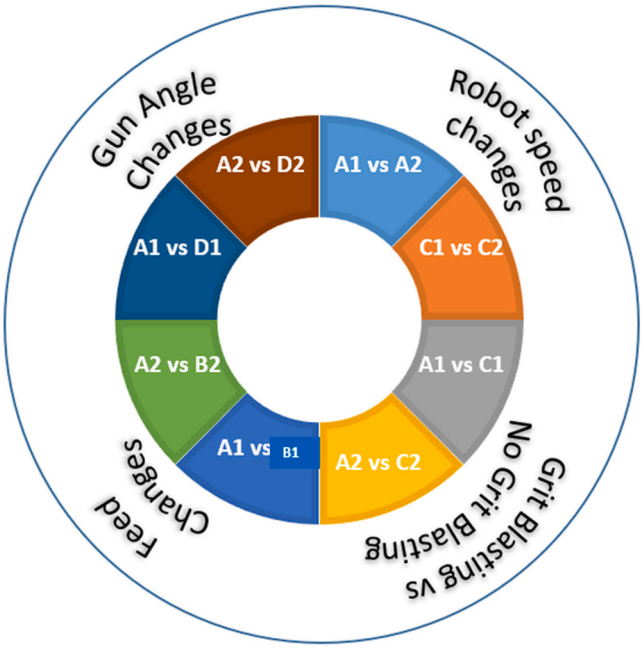

Fig. 3. Influence of correlated parameter conditions (see Table S2 in the supplementary information).

powder was used to study four variables to perform the deposition on a steel plate of thickness 2 mm, length 600 mm and width 300 mm. The plate was clamped to a bench vice with sensors mounted on the back of the plate.

To study the machine learning ability of the acoustic data, a testbed study was made to feed the model as a training dataset. This data compared the spray under two conditions using VGG-16 under two spray conditions such as in the first case, the sample substrate was grit blasted (GB) and another case where the sample was not grit blasted (NGB). A novel protocol was designed to generate acoustic data, consisting of 37.5-millisecond samples that were fed as inputs for the deep-learning classification models.

A rectangular metal plate was divided into equal halves along the length. Only the right half of the plate was grit blasted. A total of

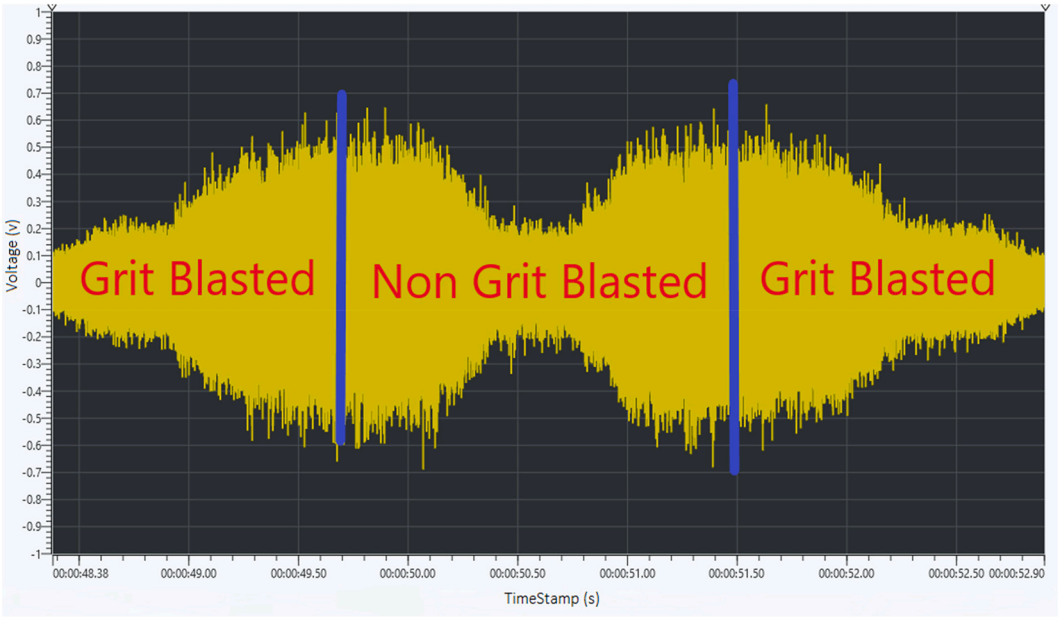

Fig. 4. Waveform during spraying on Grit Blasted (GB) and Non-Grit Blasted (NGB) areas. Robot enters the grit blasted portion first and then traverses through the NGB portion before returning to the same path but in reverse order from 50.52 s (non-grit portion first followed by grit blasted portion).

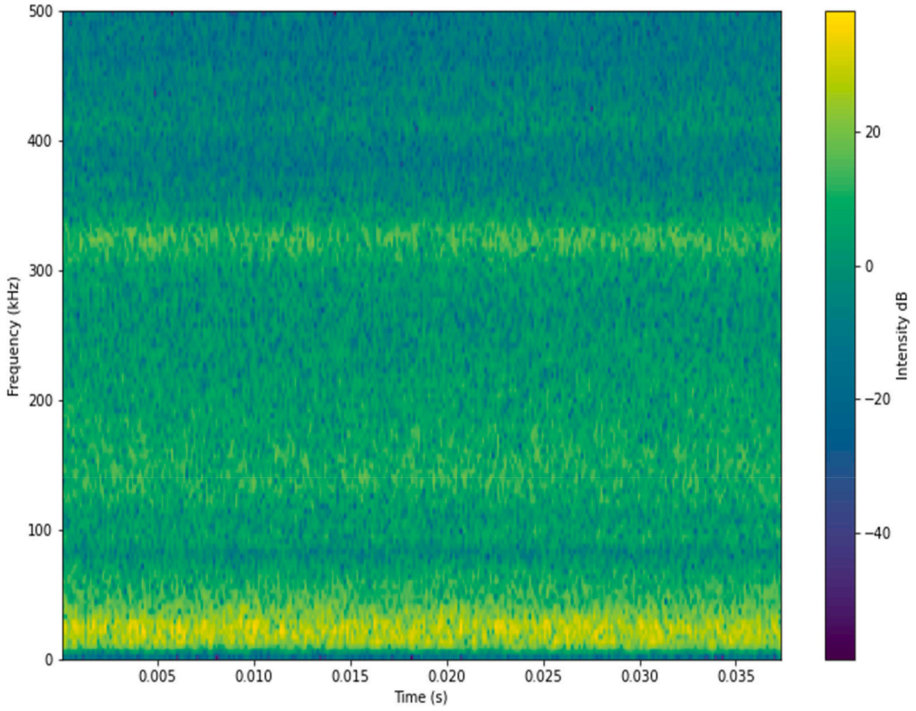

Fig. 5. Spectrograms of 37.5 ms long (a) GB chunk and (b) NGB Chunk.

five passes were conducted, with different feed rates in each pass. The voltage signals were captured via the data acquisition kit at the sampling rate of 1 MHz. The total recording was made for 58 s, where each pass generated a response acoustic band signal of approximately 4 to 5 s. Annotation for the Grit Blasted (GB) and Non-Grit Blasted (NGB) samples was done by further splitting of each band. As shown in Fig. 4, the left quarter of the signal until 49.54 s shows the acoustic spectra when the robot travels through the grit-blasted half of the plate and the second left quarter from 49.54 s until 50.52 s shows the robot travel on the non-grit blasted half of the plate. The robot returns on the same path when it encounters the non-grit portion first from 50.52 s to 51.50 s and then traverses through the grit blasted portion again from 51.50 s to 52.40 s. To split the band, the time stamps of each GB signal half and NGB signal half were analysed.

Using Python and MATLAB, the raw TDMS file was converted into wav format and chunks of wav files corresponding to the time stamps were generated. These chunks were either GB or NGB. A total of 400 chunks, each 37.5 ms long, were generated, out of which 200 were GB and 200 were NGB. Generating these chunks served two purposes: firstly, a balanced dataset of equal GB and NGB acoustic samples from the whole recording was produced. Secondly, these chunks could potentially have unique acoustic signatures, implying that in instances where an acoustic signal can possibly have signatures at smaller time intervals, more data can be produced by simply splitting the signal. Such type of data can be used in applications where acoustic signatures serve as the features for training DL models.

As discussed earlier, the Fourier-transformed frequency vs time plots are ideal for the acoustic analysis. Therefore, each chunk was fast-Fourier transformed, converting it into spectrograms. A spectrogram is the visual representation of a signal's strength at various frequencies over a time. Spectrograms also reduce the complexity of the problem by reducing an audio classification task to an image classification task. Fig. 5(a) and (b) show the spectrogram of one GB chunk with that of the NGB chunk of the same pass. The resulting spectrogram dataset was used for training three Deep Learning models - A pre-trained, tuned VGG 16, an un-trained VGG 16 and a 6-layered CNN model.

4. Results and discussions

This section discusses various time–frequency plots wherein the recording time was plotted on the Y-axis and frequency of the acoustic waves were recorded on the X-axis. The values of the colour bar in Figs. 6–13 show the magnitude of the signal acquired by the acoustic emission transducer. Considering the amplitude of the range of the values, the signal, which was recorded in Volts, was transformed into decibels (with 0 dB representing 1 Volt) to obtain a narrower scale of values. Thus, the colours can be presented to depict a smoother variation. It must be taken into account that the absolute value is not really meaningful because it depends on the position of the acoustic emission transducer, the material tested, etc. Therefore, the relative values or the changes should be considered.

The frequency bands were divided in three distinct zones namely, a strong red base band (<100 kHz), a faded yellow/teal band from 80 kHz until 380 kHz and the histogram band itself with three different colours (red, yellow and teal). The red base band was consistently observed across all trials. The base material in the form of a plate was gripped to the vice, allowing external forces to cause it to oscillate similarly to a cantilever beam. The external forces in this case were a result of the ignition from the spray gun, the exhaust vent air, robot motion and particle feed rate. Thus, the low frequency base band of < 100 kHz was recorded because of gun ignition, exhaust vent, the external noise from firing of the gas swirl gun and the gas swirling inside the gun. The faded teal band was a result of the particles bouncing back or in the air that never get deposited and will serve to improve the deposition efficiency of the coating process. The fact that the faded teal band matches with the red frequency band of the plume histogram proves that the dust cloud exists until the gun rasters itself on the substrate.

A marked difference in the shades of particle histogram between A1 and A2 was seen because of the difference in the robot speed (Fig. 6). The intensity of the particle histogram was 1 MHz in the case of titanium, but it varies with particle chemistry and the physical property. Hence, band height could be mapped to particle composition and particle size could serve as a unique identifier in a

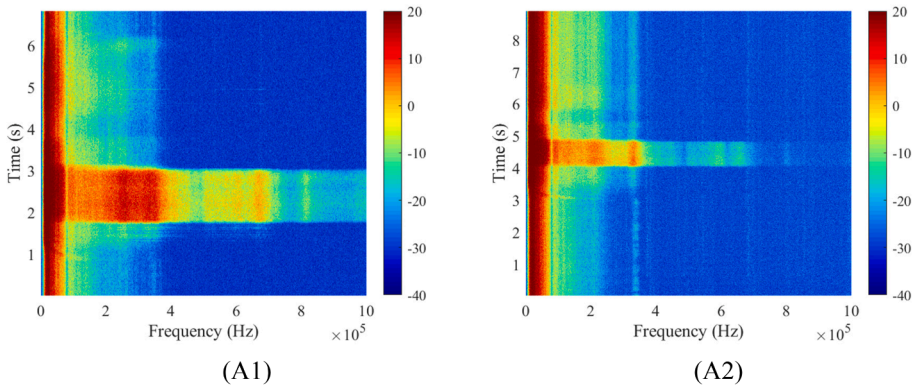

Fig. 6. Comparison of the parameters A1 and A2 with constant spray parameters and powder feed rate and only varying the robot speed (500 mm/s (A1) vs 800 mm/s (A2)).

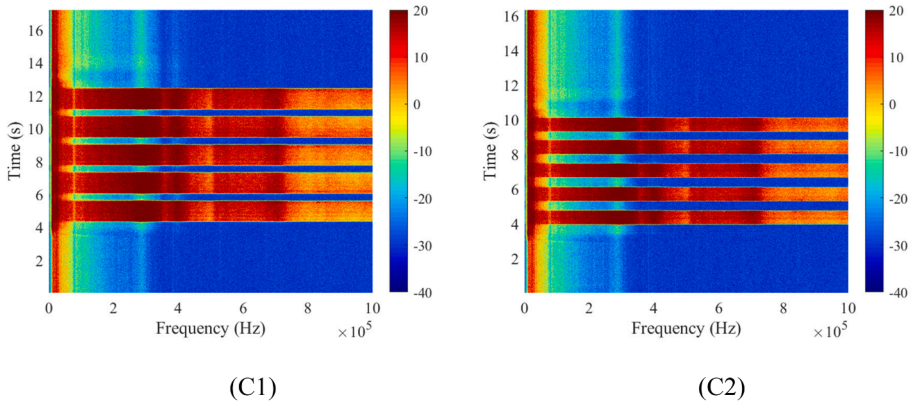

Fig. 7. Comparison of parameters C1 and C2 (GB) with a powder feed rate of 15 g/min and only varying the robot speed (500 mm/s vs 800 mm/s).

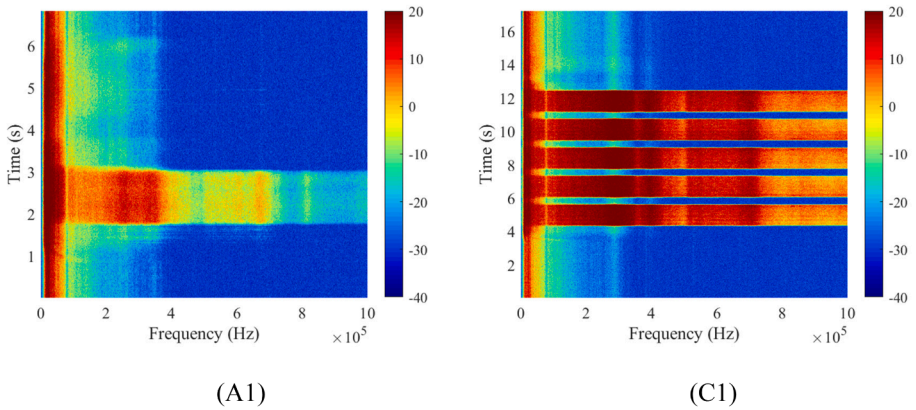

Fig. 8. Comparison of parameters A1 (NGB) and C1 (GB) with a power feed rate of 5gm/min and 15 g/min respectively but with identical robot speed of 500 mm/s in both cases.

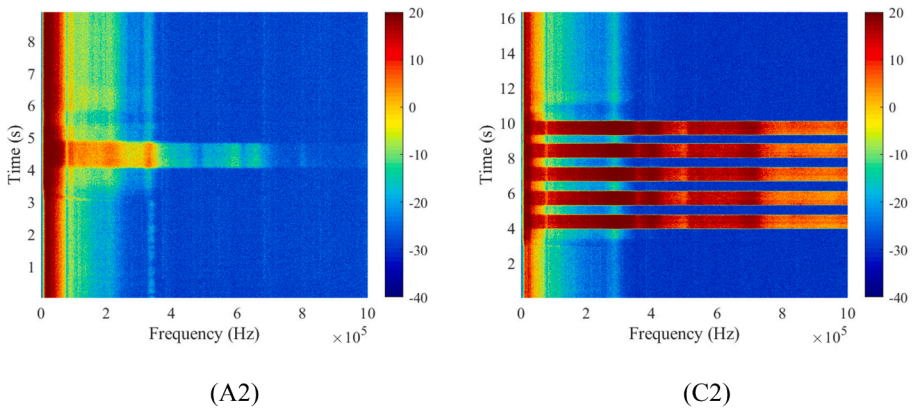

Fig. 9. Comparison of parameters A2 (NGB) vs C2 (GB) with a powder feed rate of 5 g/min and 15/min respectively but with identical robot speed of 800 mm/s in both cases.

manufacturing setting. The time taken by the gun to move over the plate (2–3 s in case of A1 and 4–5 s in case of A2) manifests itself through the width of the frequency histogram spectrum. The red band in the powder histogram from 80 to 380 kHz reveals that about 30 % of particles gets deposited with high impact. These particles adhere to the substrate and provide the needed bond strength to keep the coating intact with the substrate. The yellow band from 380 kHz to 700 kHz could have unmelted parts and partially impact the substrate and the teal bands above it were either unmelted or particles that could lead to more porosity in the coating. For the same

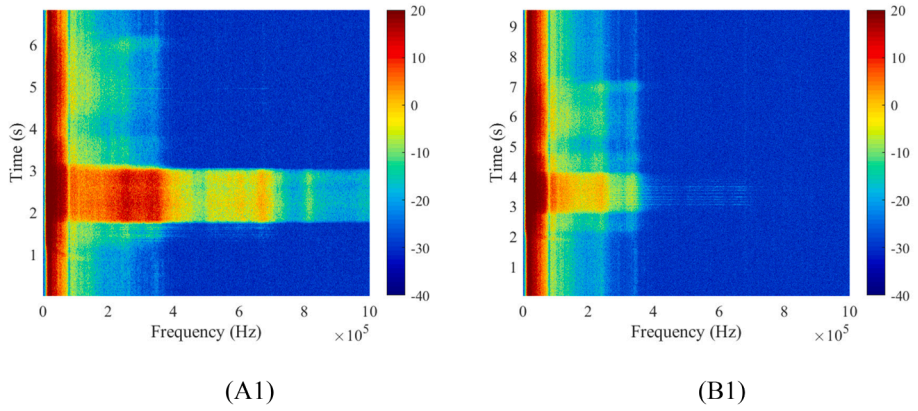

Fig. 10. Comparison of parameters A1 (NGB with powder) and B1 (NGB with no powder) at identical robot speeds of 500 mm/s.

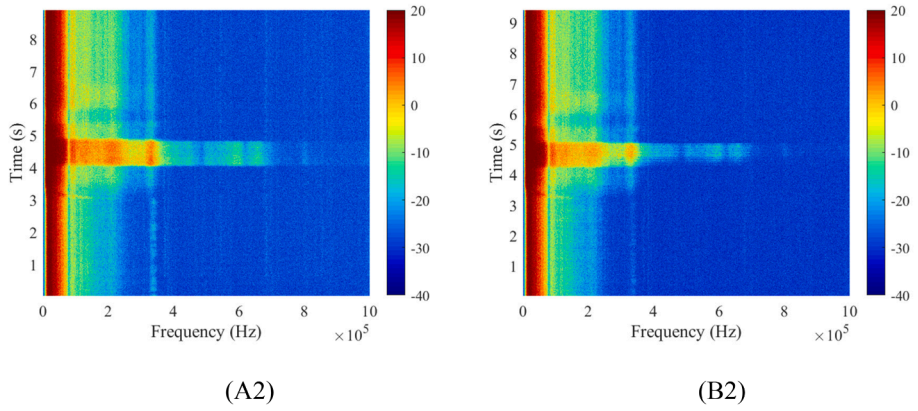

Fig. 11. Comparison of parameters A2 (NGB powder) and B2 (NGB no powder) at identical robot speeds of 800 mm/s.

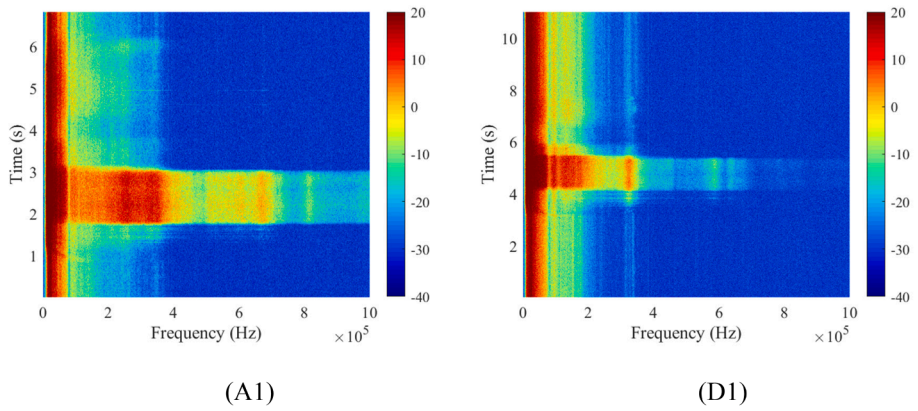

Fig 12. Comparison of parameters A1 (NGB powder) with that of D1 (gun off angle, GB powder) at identical robot speeds of 500 mm/s.

setup at A2, the gun-base material interaction shrunk by 25 % which was a good indication that the robot speed has increased from 500 mm/s to 800 mm/s. As a result of the lower dwell time of the gun on the base material in the latter case (A2), it is to be seen that the yellow band wave generation was non-existent and the teal band extends from 380 kHz to 1 MHz due to less impacting particles and thereby less deposit volume on the substrate. Only one pass was given as the substrate was not blasted and there would be no adhesion of particles to the substrate even with multiple passes. The study was done to simply capture what can be expected as a signature when the surface was not properly grit blasted.

It was found that the acoustic waves showed a different sequence of events from turning on the exhaust, switching on the power

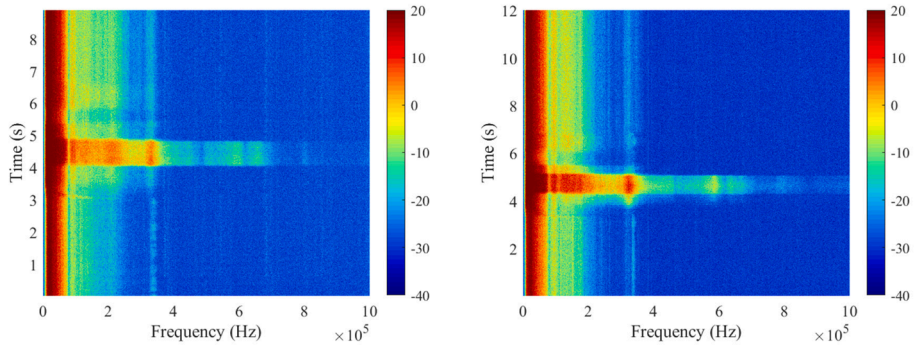

Fig. 13. Comparison of parameters A2 (NGB powder with gun normal to the surface,) with that of D2 (GB powder with gun off angle) at identical robot speeds of 800 mm/s.

supply, striking the arc between the anode and cathode and the full development of the arc, the gas swirl, the powder feed flow and the movement of the robot over the base material. They also propagate differently according to their frequency. Two sensors were placed to ensure that the accuracy of the frequency of waves generated is repeatable. The depth of the propagation was kept uniform by selecting a base material with uniform thickness (2 mm). Low frequency events up to 50 kHz could be attributed to the exhaust flow. The event 50–75 kHz was due to turning on the power supply and the gas swirling through the anode and the arc striking. Future studies might benefit from employing frequency filters to isolate these events, offering insights into ideal frequency ranges for the aforementioned events. However, this was not in the scope of this study.

With grit blasting and 15 g/min powder, it was expected to have a dense generation of frequencies up to 450 kHz which was further confirmed (see Fig. 7). Five bands revealed 5 passes and the gap between the bands showed the robot movement in the air to avoid overheating of the base material. It must be noted that every pass adds material to the substrate and the grit blasting and spray parameters including powder flow have been so consistent that all 5 repeated pass histograms generated identical acoustic frequencies, and this would serve as a visual benchmark for any process anomalies for a frozen process with a predetermined material and process. The width differences of the bands between C1 and C2 revealed that the robot moved faster when the width is shorter and slower when the width is higher. Since, such unique bands are assigned, it helps to create unique CNN/ANN models to quantify the flow rate of the powder. This quantification can be used to loop to the process control and set real-time changes to gas flow controllers and feeders to meet the powder plume characteristics.

Fig. 8 revealed that grit blasting triggered high frequency acoustic waves especially with frequencies in the range of 400 kHz to 1 MHz band than in case of A1. Thus, digital contrast between a grit blasted vs non grit blasted surface could be made available for the models to learn and create a machine learning paradigm. Fig. 9 is additional evidence to the fact that a visual deviation in the process could be revealed using acoustic emission patterns. The plot shown in Fig. 10 show that when there is a collective anomaly with improper surface preparation and the powder feed malfunctioning, it could lead to very low frequency faded bands and will serve to digitize the caution boards. If powder flow is stopped, it stops generating the $>$ 450 kHz, thereby clearly distinguishing the powder vs no powder situations. Fig. 11 also reveals the same pattern with only difference being that the robot speed was higher in the latter case.

Like Fig. 10, Fig. 11 portrays a consistent trend: even at elevated robot speeds, a poorly prepared or non-grit blasted (NGB) surface combined with the absence of powder does not enhance the prospects of superior coating quality. Fig. 12 revealed that the orthogonal gun angles (A1) showed clear signal intensities even without grit blasting compared to off angle spray. While it is inevitable to avoid off angles from complex geometries, the presence of low frequency bands in off angle spray against a wide-ranging array of frequencies generated with orthogonal spray conditions serve to differentiate the two and therefore gives opportunity for optimising the gun angle.

Fig. 13 showed similar observations for increased robot speeds although it was found that the signal frequencies of off angle spray were captured better with high robot speed and therefore inevitable off angle spray processes could be made better with increased robot speeds. Comparison of parameters A2 and D2 show that off angle spray is much like a NGB surface and will lead to poor deposition efficiency and thickness build-up rate. This study helped to provide a comparison of interrelations between critical spray parameters and how they can affect the acoustic frequency wave generation. The study was aimed at proving that acoustic data generation could successfully digitize a manufacturing process that has largely remained a skilled intensive manual process.

The effect of one variable and the influence of one to more variables combined is a quite complex thing to understand and therefore, it is difficult to identify the root cause of the coating failure. The definition of a failed coating depends on the specification that each coating must comply with. For example, a TBC topcoat with a porosity range of 5–10 % could end up being $>$ 10 % or less than 5 % thereby rendering the coating as failed and causing it to rework. If this can be mapped while the coating deposition is in process and corrective action could be taken, then we can save the entire coating from being stripped and reworked. This is where the acoustic emission data would help creating a unique signature of what will constitute a low porosity or a high porosity regime. Every single deviation or anomaly in thermal spray could be mapped and a standard acoustic wave pattern could be created while the particles are impacting the substrate. The scope of the work could be confirmed to thin coatings of the order of 100–200 μm. Thick coatings of the

order of 1 mm will need more detailed studies and are beyond the scope of this work.

Consequently, acoustic data collected by grit blasting and non-grit blasting at 90° angle was used to train three deep-learning models and compare their performances.

5. DL based binary classification models for thermal spray acoustic digital data

As discussed earlier, a Convolutional Neural Network (CNN) model may provide exemplary results in image classification tasks. The standard CNN architecture is composed of three major types of layers: Convolutional layer, Pooling layer and fully connected layer. A convolutional layer is the foremost and fundamental layer, where all the major computation occurs. It receives the input data, typically as an image, which is scanned by a feature detector, also known as a kernel or a filter which checks for features. This process is known as convolution. A feature map is generated after the whole image has been swept by the feature detector. Pooling layers reduce the number of parameters from the input either by selecting the pixel with the maximum value or by calculating the average of all the pixels present. Thus, these layers help to reduce the complexity of data, mitigate the risk of overfitting and improve the efficiency of the algorithm. Fully connected layers are interconnected in the sense that the inputs from the layer are connected to every unit of the upcoming layer. These layers flatten the output of the pooling and convolutional layers into a single vector. The last fully connected layer represents the output of the network. The architecture is shown in Fig. 14.

Two aspects central to efficient CNN models are the amount of available data and the computational expense of the model. In a thermal spray environment, gathering large amounts of data is often very time-consuming and poses monetary constraints. This task becomes more unsuitable in anomaly detection tasks where data from production-failure scenarios is unrealistic to produce. Even if large amount of data is captured, a computationally intensive CNN model will require multiple processing units to learn and train to produce reliable results. In order to eliminate the expensive and time-consuming exercise of training CNN models from scratch each time, a transfer learning approach can be used. Transfer learning is a popular method which utilizes knowledge learned from different but related tasks to solve a specific task. It is most applicable in situations where data availability is limited, and data from two tasks: Source and target, are similar in nature. To achieve transfer learning functionally, pre-trained neural network models can be used. Such model architectures are trained on large and complex datasets such as ImageNet, which contains millions of labelled images, allowing them to extract highly abstract and complex features from input data. VGG 16 is one such model; it has 13 convolutional layers, followed by 3 fully connected layers.

To demonstrate the effectiveness of implementing transfer learning, the study implemented three DL models for a binary classification task. First one was a VGG 16 model, pre-trained on ImageNet database. The second model was VGG 16, with all its layers trainable and hence untrained. The third model was a custom built 6 layered CNN model. The target dataset used are the spectrogram images of Grit and Non-Grit blasted surface acoustic emissions, discussed in section 3.

The training of models comprised of:

1. Data preparation: Initial aspects are described in the research methodology action, involving the collection of grit and non-grit acoustic data, its trimming and the conversion of acoustic dataset to the spectrogram dataset. Subsequently, the spectrogram dataset was labelled with two classes- Grit (GB) and Non-Grit (NGB), each class having 200 images. After the random train-test split of data, the images were label encoded to finalize the input image data.

2. Model Creation and Tuning: Architecture of the three models were defined. The hyper-parameters were passed as arguments based on hyper-parameter tuning. To tune the pre-trained VGG 16 for our dataset, first 11 layers were frozen while the rest were unfrozen. This step ensured that the pre-trained model incorporated the target dataset features into its training. The fully un-trained VGG 16 had all its layers unfrozen and hence fully trainable. Custom layers were added to both the models for additional training on our dataset. The 6 layered CNN model had the same input shape as the VGG models, and custom fully connected layers were added. These layers included dropout layers to ensure mitigation of overfitting.

3. Hyper-Parameters Tuning: GridSearchCV was used to ensure optimal hyper-parameters for the models training. 10-fold Cross Validation step was also passed as an argument to the search process. Addition of parameter space in GridSearchCV increases resource constraints, hence other methods such as RandomSearchCV can be adopted to bypass high GPU and memory requirements.

4. Evaluation metric: Since the dataset was balanced, accuracy was taken as the evaluation metric. Other metrics, such as the F1 score, ROC-AUC, can be implemented to adapt with any imbalanced dataset attributes.

The Pre-Trained (PT) VGG 16 model results shown in Fig. 15(a) achieved a test accuracy score of 85 % in 200 epochs, followed by

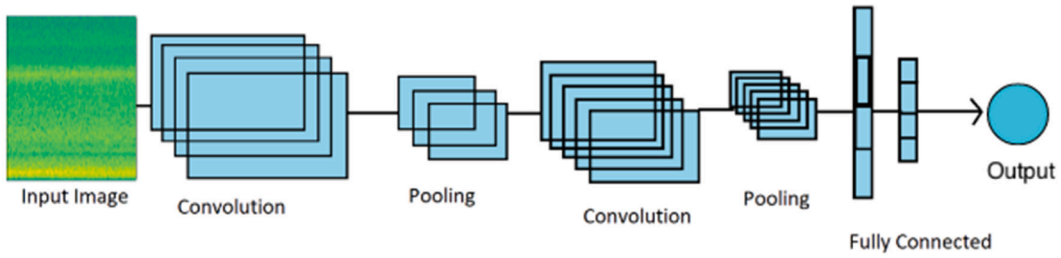

Fig.14. Standard CNN architecture with an input of 37.5 ms long spectrogram image.

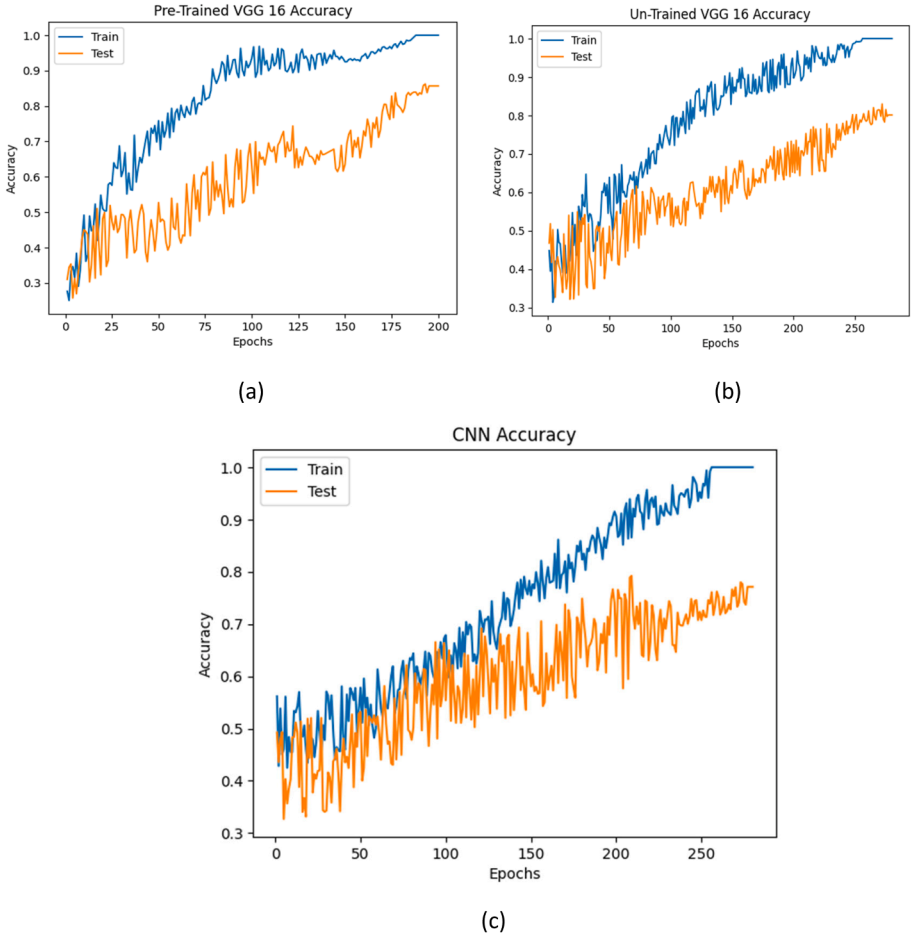

Fig.15. Accuracy graphs of (a) Pre-Trained VGG 16, (b) Un-Trained VGG 16 and (c) 6 layered CNN.

Un-Trained (UT) VGG 16 shown in Fig. 15(b) which achieved an accuracy of 80 % in 280 epochs, while the 6 layered CNN achieved an accuracy of 77 % in 278 epochs (see Fig. 15(c)).

The fluctuations in the graphs are due to smaller batch sizes, learning rates and usage of Stochastic Gradient Descent (SGD) optimisation algorithm. These parameters were decided based on minimal GPU and memory requirements along with the diminutive nature of the data. The 6 layered CNN, in comparison to the VGG 16 models, showed more drastic fluctuations due to its relatively

Table 3
Use case comparison of a custom CNN with VGG 16 along different criteria.

Dimension	VGG 16	Custom CNN
Relation between tasks / processes	Useful in correlated tasks, offers reduced training time and economical resource consumption. Essential in production failure scenarios. Note- Tuning and addition of custom layers required to increase effectiveness.	Useful in unrelated tasks. Can be tailored for a specific task and is less constrained in terms of core-architectural modifications. Note- Can serve as a primary transfer learning model itself for subsequent related processes.
Data Availability	Given domain adaptation, it can work well with training small and large datasets, especially with intricate features. Note - More prone to overfitting in smaller datasets.	Works well with larger datasets. Smaller datasets are more prone to overfitting. Note- A less complex and small architecture can work well with small and uncomplicated datasets.
Tuning and optimization steps	• Unfreezing last few layers and addition of custom layers at the end. • Hyperparameter tuning can be computationally expensive due to larger number of hyperparameters. • The core design is optimized with regularization techniques and parameter initialization. • In case of limited training data, data augmentation is always useful in prevent overfitting.	• Changes in architecture design such as number of layers and filters, type of pooling layers, activation functions, etc. • Hyperparameter tuning using GridSearch, RandomSearch, genetic algorithm or other techniques. • Regularization techniques like L1 or L2, dropout layers, etc. should be done to mitigate overfitting. • Data augmentation is more effective in case the architecture is deep and complex.

lesser complexity and optimization.

The UT VGG 16 graph indicates sensitivity to the training and test data, but due to additional optimisations in the core architecture it offers quicker training and slightly better performance than the conventional CNN. In learning more intricate features, the pre-trained weights of the PT VGG 16 give an edge over the UT VGG 16, hence the quicker training and greater accuracy of the PT VGG 16 model. To prevent overfitting, regularization techniques and early callbacks were implemented in all the models.

While the results illustrate the superiority of the transfer learning approach, various factors would govern the applicability of a DL model in an industrial environment. The effectiveness of Transfer Learning is gauged by the relation of the pre-trained task and the target task. If the two tasks are highly unrelated, the pre-learnt weights and features will not align well with the requirements, thus nullifying the benefit of reduced training time. In such a case, custom built CNN networks can prove to be more competent, as their architecture can be tailored to the requirements of the task. Their capability is amplified in cases where images have generic or high level features, thus enabling less complex models to train well and avoid overfitting. Whereas if some relation exists between the pre-learnt tasks and the target task, transfer learning can offer major advantages. Further detailed comparisons and use cases of these models are elaborated in Table 3.

From a future perspective, the results convey two significant pathways to a potential advancement in the implementation of Machine Learning-based models in the manufacturing domain. Firstly, acoustic emissions can serve as the primary information source in a manufacturing process. As discussed earlier in the paper, changes in the critical parameters of the spraying process produce characteristic frequencies that are unique to that parameter. These characteristic frequencies can be visualised by the spectrograms in the form of varying intensities at various frequencies. Fig. 5 show the difference in the intensities of the acoustic signals from the grit-blasted portion vs the non-grit-blasted portion in the same pass. These visualisations not only serve an intuitive sense to the user but also serve as the input for image-based classification models. The need for expensive, high-quality and high-maintenance image-capturing systems to implement Machine Learning-based automation can be replaced by simple acoustic measuring devices, since these acoustic measurements can be converted to spectrograms and subsequently provide a similar level of features for an image-based CNN model to train as an image would provide. It is important to mention that the results of the study are applicable to the domain of process parameter monitoring and to the processes where characteristic acoustic signatures can be captured. In an industrial setting, data cleaning and filtering techniques will be required to remove noise and unnecessary data from the raw acoustic data. Unique acoustic signatures corresponding to the defects can labelled, converted into spectrograms and used in a CNN model. Hence a future scope of this study's findings into other areas of the manufacturing industry is also feasible.

Secondly, the study affirmed the efficacy of real-time implementation of transfer learning. In addition to the weights already learned from the ImageNet database, the model was able to train quickly than a conventional CNN on the lab recorded spectrogram dataset. In a production environment, although changing the parameters of a process will alter the process dynamics, transfer learning-based image classification models can adapt and train quickly to give accurate results. Hence, pre-trained CNN models can become more viable for real-time process monitoring applications while being less resource intensive as compared to a conventional untrained CNN model.

6. Conclusions

Thermal spraying is a surface manufacturing process used in various engineering sectors to produce components that enables swift operations in extreme environments. Digitalisation of thermal spraying process using non-invasive means continues to pose immense challenges. Previous attempts, as noted, largely depended on IR cameras and particle state sensors to capture real-time data about the powder particles in the plasma state. Such methods, however, fall short of facilitating real-time controls essential for the manufacturing process..

In this study, data gathered from process anomalies have been presented as a digital display dashboard for robot speed, powder flow, grit blast and off angle impact changes. We have successfully created a transfer learning for grit and no grit substrate coated with thermal spray and allowed the transfer learning model to learn and predict the grit blasting and no grit blasting conditions as accurately as possible. Thus, this model could be extended to train and predict all such anomalies that happen during the thermal spray manufacturing process.

This novel study provides a disruptive approach in obtaining the in-flight data during thermal spraying through acoustic emission sensing to enable real-time intervention during manufacturing. Our suggested approach can help to correct the process anomalies to serve as a pathway to digitization of thermal spray. The sensitivity of the acoustic spectrum to respond to the process changes during thermal spray such as the feed rate, robot speed, surface preparation and off angle spray were investigated and the findings we report here constitute the first step in digitization of thermal spray manufacturing. We also evaluated a testbed to train the acoustic data into a transfer learning model using Convoluted Neural Networks (CNN). The primary learnings from this study were that the changes in robot speed changes, off angle deposition, powder feed interruptions, non-grit blasted surfaces are sensitive to the acoustic frequency and this information was used and analysed to understand various correlations between spraying parameters and conditions.

In conclusion, this research paves the way for a transformative approach to thermal spray manufacturing, anchoring on the synergy of acoustic emissions and advanced machine learning paradigms.

Data Repository: The raw data used to generate the results in this work will be available based on the reasonable request to the corresponding author.

Declaration of competing interest

The authors declare that they have no known competing financial interests or personal relationships that could have appeared to influence the work reported in this paper.

Data availability

Data will be made available on request.

Acknowledgements

All authors acknowledge the financial support provided by the UKRI via Grants No. EP/S036180/1, EP/W033178/1 and EP/T024607/1, Hubert Curien Partnership award 2022 from the British Council and the International exchange Cost Share award by the Royal Society (IEC\NSFC\223536). AT is thankful to the Royal Academy to support him with the Research Chair award (RCSRF1718\5\41). AM and IV also gratefully acknowledge the financial support given by the Eusko Jaurlaritza via Grants No. KK-2020/00063 (SUSIE) and KK-2022/00080 (MINAKU)

Appendix A. Supplementary data

Supplementary data to this article can be found online at https://doi.org/10.1016/j.ymssp.2023.111030.

References

[1] V. Viswanathan, N.K. Katiyar, G. Goel, A. Matthews, S. Goel, Role of thermal spray in combating climate change, Emergent Materials (2021) 1–15.
[2] N.H. Faisal, A. Prathuru, R. Ahmed, V. Rajendran, M. Hossain, V. Venkatachalapathy, N.K. Katiyar, J. Li, Y. Liu, Q. Cai, Application of thermal spray coatings in electrolysers for hydrogen production: advances, challenges, and opportunities, ChemNanoMat (2022) e202200384.
[3] C.U. Hardwicke, Y.-C. Lau, Advances in thermal spray coatings for gas turbines and energy generation: a review, J. Therm. Spray Technol. 22 (5) (2013) 564–576.
[4] A. Vardelle, C. Moreau, J. Akedo, H. Ashrafizadeh, C.C. Berndt, J.O. Berghaus, M. Boulos, J. Brogan, A.C. Bourtsalas, A. Dolatabadi, The 2016 thermal spray roadmap, J. Therm. Spray Technol. 25 (2016) 1376–1440.
[5] K. Malamousi, K. Delibasis, B. Allcock, S. Kamnis, Digital transformation of thermal and cold spray processes with emphasis on machine learning, Surf. Coat. Technol. 433 (2022), 128138.
[6] X. Zhao, C. Li, S. Li, H. Jiang, X. Han, Time-varying evolutionary mechanism analysis of the multiphase flow during high-velocity oxygen-fuel (HVOF) thermal spraying WC-12Co particle, Surf. Coat. Technol. 461 (2023), 129435.
[7] X. Gao, C. Li, X. Han, X. Chen, X. Zhao, Numerical simulation and parameter sensitivity analysis of multi-particle deposition behavior in HVAF spraying, Surf. Coat. Technol. 441 (2022), 128569.
[8] X. Zhao, C. Li, S. Li, X. Han, H. Jiang, Mechanism study on the influence of combustion models and spray gun geometric parameters on high-velocity oxygen-fuel (HVOF) thermal spraying, J. Manuf. Process. 98 (2023) 173–185.
[9] W. Zhang, S. Sampath, A Universal Method for Representation of In-Flight Particle Characteristics in Thermal Spray Processes, J. Therm. Spray Technol. 18 (1) (2009) 23–34.
[10] N. Faisal, R. Ahmed, R. Reuben, B. Allcock, AE monitoring and analysis of HVOF thermal spraying process, J. Therm. Spray Technol. 20 (2011) 1071–1084.
[11] S. Deng, Z. Cai, D. Fang, H. Liao, G. Montavon, Application of robot offline programming in thermal spraying, Surf. Coat. Technol. 206 (19–20) (2012) 3875–3882.
[12] J. Agapakis, T. Hoffman, Real-time imaging for thermal spray process development and control, J. Therm. Spray Technol. 1 (1992) 19–25.
[13] X. Li, S. Siahpour, J. Lee, Y. Wang, J. Shi, Deep learning-based intelligent process monitoring of directed energy deposition in additive manufacturing with thermal images, Procedia Manuf. 48 (2020) 643–649.
[14] J. Yang, S. Li, Z. Wang, H. Dong, J. Wang, S. Tang, Using deep learning to detect defects in manufacturing: a comprehensive survey and current challenges, Materials 13 (24) (2020) 5755.
[15] J. Lee, J. Singh, M. Azamfar, V. Pandhare, Industrial AI and predictive analytics for smart manufacturing systems, Smart Manufacturing, Elsevier2020, pp. 213-244.
[16] B. Maschler, H. Vietz, H. Tercan, C. Bitter, T. Meisen, M. Weyrich, Insights and Example Use Cases on Industrial Transfer Learning, Procedia CIRP 107 (2022) 511–516.
[17] H. Tercan, A. Guajardo, T. Meisen, Industrial Transfer Learning: Boosting Machine Learning in Production, 2019 IEEE 17th International Conference on Industrial Informatics (INDIN), 2019, pp. 274-279.
[18] K. Simonyan, A. Zisserman, Very deep convolutional networks for large-scale image recognition, arXiv preprint arXiv:1409.1556 (2014).
[19] L. Zhao, L. Kang, S. Yao, Research and application of acoustic emission signal processing technology, Ieee Access 7 (2018) 984–993.
[20] M.G. Droubi, N.H. Faisal, F. Orr, J.A. Steel, M. El-Shaib, Acoustic emission method for defect detection and identification in carbon steel welded joints, J. Constr. Steel Res. 134 (2017) 28–37.